Fractionation of Ligusticum Chuanxiong by Adsorption in Supercritical Carbon Dioxide

ARTICLE *in* INDUSTRIAL & ENGINEERING CHEMISTRY RESEARCH · OCTOBER 2012

Impact Factor: 2.59 · DOI: 10.1021/ie301274x

4 AUTHORS, INCLUDING:

Dong Hui Zhang

Tianjin University

12 PUBLICATIONS **51** CITATIONS

SEE PROFILE

I&EC research
Industrial & Engineering Chemistry Research

Article

pubs.acs.org/IECR

Fractionation of *Ligusticum* Chuanxiong by Adsorption in Supercritical Carbon Dioxide

Zhihui Hu,[†] Donghui Zhang,[†,*] Jixiao Wang,[†] and Motonbu Goto[‡]

[†]Chemical Engineering Research Center, State Key Laboratory of Chemical Engineering, School of Chemical Engineering and Technology, Tianjin University, Tianjin 300072, People's Republic of China

[‡]Bioelectrics Research Center, Kumamoto University, Kurokami 2-39-1, Kumamoto 860-8555, Japan

ABSTRACT: An experimental and simulated study of the fractionation of *Ligusticum* chuanxiong via adsorption in supercritical carbon dioxide (SC-CO_2), using silica gel as the adsorbent, was conducted. Adsorption equilibrium and adsorption dynamic data were obtained from experiments conducted at 8.8 MPa and 323.15 K. The adsorption isotherms can be represented by the Extended Langmuir 1 isotherm equation. Effect of the flow rate of the strippant was studied, and the regeneration became more complete and occurred more quickly as the flow rate of the strippant increased. Highly concentrated fraction of lactone was obtained for the desorption step and the recovery of it reached 85%. A mathematical model simulated the behavior of the process well, and the amount of adsorbed components on the adsorbents was predicted graphically.

1. INTRODUCTION

Ligusticum wallichii (commonly known as chuanxiong) is a traditional Chinese medicine (TCM) that is commonly used for cardiovascular protection, atherosclerosis, and hypertension in China.[1] *Ligusticum* chuanxiong contains many complex constituents with only a low amount of bioactive ingredients. Sorting out and identifying these ingredients is an important task in biochemical, pharmaceutical, and clinical research. Many techniques have been used to separate the components in TCMs, such as thin-layer chromatography (TLC),[2] gas chromatography (GC),[3] high-performance liquid chromotography (HPLC),[4] capillary zone electrophoresis,[5] and two-dimensional liquid chromatography.[6]

Separating the components in TCMs using adsorption in supercritical carbon dioxide (SC-CO_2) is an attractive method, because CO_2 is nontoxic, nonflammable, odorless, tasteless, inert, and inexpensive. Over the past decade, adsorption in SC-CO_2 has been reported by many researchers.[7−21] Bracey et al.[8] separated aqueous mixtures of fructose and glucose in SC-CO_2, by using activated carbon as the adsorbent. The adsorption step was conducted at 8.3 MPa and the desorption step was conducted at 15.2 MPa with the SC-CO_2 containing small amounts of ethanol. Iwai et al.[10−13] studied the adsorption behavior of an isomeric mixture of 2,6- and 2,7-dimethylnaphthalene in SC-CO_2 using a NaY-type zeolite as the adsorbent and the examined the effects of temperature and pressure on the adsorption behavior. Goto et al.[7,16,17] evaluated the adsorptive separation process for citrus oil in SC-CO_2 using silica gel. The citrus oil was passed through an adsorber at 8.8 MPa, and then adsorbent was regenerated with SC-CO_2 at 19.4 MPa.

Aspen Adsim adsorption software (by Aspen Technology, Inc.) is often used to select optimal adsorbents, design better adsorption cycles, and improve general plant operations. A wide range of industrial gas and liquid adsorption processes have been simulated and optimized successfully with Aspen Adsim.[22−25] Barcia et al.[22,24] used Aspen Adsim to simulate the dynamic adsorption behavior of the C5−C6 fraction in a nonisothermal and nonadiabatic adsorbent bed. The simulation data gave a good description of the experimental data. Choi et al.[25] successfully used Aspen Adsim to simulate a multibed pressure swing adsorption process for producing high-purity hydrogen from synthesis gas.

Although a review of the previous studies on adsorption separation of TCM in supercritical fluid chromatography (SFC) and adsorption process simulation with Aspen Adsim is presented above, the review shows that, so far, no hybrid extraction−adsorption has been developed in the literature to separate components from *Ligusticum* chuanxiong in SFC. Therefore, our objective is to develop an extraction−adsorption combined process to sort active ingredients from *Ligusticum* chuanxiong. The process involves three fundamental steps: (1) the extraction step, where the components were first dissolved into SC-CO_2 to form the feed; (2) the adsorption step, where the feed is passed through an adsorbent bed and the component of interest is preferentially adsorbed from the feed onto the bed; and (3) the regeneration step, where the adsorbed components are removed from the adsorbent using SC-CO_2 that contains some strippant, such as ethanol. In addition, the Aspen Adsim liquid adsorption model was used to simulate this process to understand the adsorption−desorption behavior of components on a silica gel adsorbent in SC-CO_2. SC-CO_2 containing 5% (molar mass) ethanol was used to elute the components of *Ligusticum* chuanxiong adsorbed on the adsorbent.

2. EXPERIMENTAL SECTION

2.1. Materials. Silica gel was obtained from Dalian Haixin Chemical Industrial Co., Ltd., and the physical properties of the

Received: May 16, 2012
Revised: October 16, 2012
Accepted: October 19, 2012
Published: October 19, 2012

dx.doi.org/10.1021/ie301274x | *Ind. Eng. Chem. Res.* 2012, 51, 14496−14502

adsorbent are shown in Table 1. Carbon dioxide with a purity of 99.9% was used. *Ligusticum* chuanxiong, purchased from Tianjin Pharmacy Company (Tianjin, PRC), was ground using a mixer−grinder and then was sieved through a mesh screen (80). Ferulic acid (≥98% by HPLC), z-ligustilide (≥99% by HPLC), ligustrazine (≥98% by HPLC), and senkyunolide I (≥98% by HPLC) were acquired from China Standard Material Center (Beijing, PRC).

Table 1. Physical Properties of the Silica Gel Material

parameter	value
pellet diameter, d_p	1.0×10^{-3} m
pellet porosity, ε_p	0.35 $cm^3\ g^{-1}$
macropore radius, r_{pore}	3.0×10^{-9} m
surface area, s	650 $m^2\ g^{-1}$
apparent density of the pellet, ρ_s	0.789×10^3 kg m^{-3}
density of fluid phase, ρ_l	481 kg m^{-3}
critical temperature of CO_2, T_C	304.41 K
critical pressure of CO_2, P_C	7.29 MPa

2.2. Measurement of the Breakthrough Curve. A schematic diagram of the experimental apparatus is shown in Figure 1 (purchased from Applied Separations, Inc.). It consisted of a mixing column, an adsorption column, an ethanol vessel, and a CO_2 cylinder. The mixing column (32 mL) was filled with 10.5 g *Ligusticum* chuanxiong, and the adsorption column (10 mL) was packed with 4.46 g of silica gel adsorbent. Both columns then were installed in the constant temperature oven. After being cooling in a bath at ∼273 K, the CO_2 was simultaneously compressed to the predetermined pressure (8.8 MPa) and heated to the predetermined temperature (328.15 K). Next, solenoid valves S1, S2, and S3 were opened while the others remained closed, and the SC-CO_2 passed through the mixing column and dissolved the *Ligusticum* chuanxiong to form the feed. The feed then passed through the adsorption column for the adsorption step. The pressure was controlled by two back-pressure regulators (BPRs), and BPR1 and BPR2 were set at 8.8 MPa. Breakthrough curve analyses were carried out for various concentrations of feed, where the flow rate of CO_2 was ∼6.8×10^{-8} m^3/s (8.8 MPa, 328.15 K). The effluent was expanded to ambient pressure using a BPR, and then collected in a receiving bottle. The flux of the expanded gas was measured by a wet gas totalyzer.

In the desorption step, solenoid valves S1, S4, S5, and S6 were opened while the others remained closed, and a mixture of ethanol and SC-CO_2 passed through the adsorber column to elute the components that had adsorbed on the adsorbent.

Ligusticum chuanxiong contains many components, such as ferulic acid, ligustrazine, senkyunolide I, levistolide I, neocnidilide, z-ligustilide, neocnidilide, and 3-butylidenephthalide. In this work, ferulic acid, z-ligustilide, ligustrazine, and senkyunolide I were chosen as target components.

2.3. Analysis. The effluent was dissolved in ethanol and then analyzed via high-performance liquid chromatography (HPLC), using a LabAlliance HPLC system with an Agilent symmetry C_{18} column (5 μm, 250 mm × 4.6 mm). Detection was by measuring UV adsorption at 297 nm. The mobile phase consisted of 30% aqueous acetic acid (0.05%, v/v) and 70% methanol (v/v).[27] The flow rate was 0.6 mL/min, the injection volume was 20 μL, and the column temperature was 298.15 K.

2.4. Modeling. To obtain reliable predictions, the processes were modeled and simulated using Aspen Adsim adsorption software. The mathematical model used in this work was based on the following approximations: (i) the fluid phase is ideal, (ii) the bed is under isothermal and adiabatic conditions, (iii) the bed is initially filled with SC-CO_2, (iv) the Upwind Differencing Scheme 1 (UDS1) discretization method is available for liquid adsorption processes and the number of nodes is 20, (v) the flow is modeled as convection with no dispersion and the pressure drop is neglected, (vi) the superficial velocity is constant, (vii) the separation resistances are lumped as a single overall factor, whereas the mass transfer driving force is a linear function of the solid-phase loading, (viii) the adsorption equilibrium is described by an Extended Langmuir 1 model.

The mass balance in the liquid phase includes four parts—the effect of the axial dispersion, the convection term, the liquid-phase accumulation term, and the rate of flux to the solid surface—and is represented by the following equation:

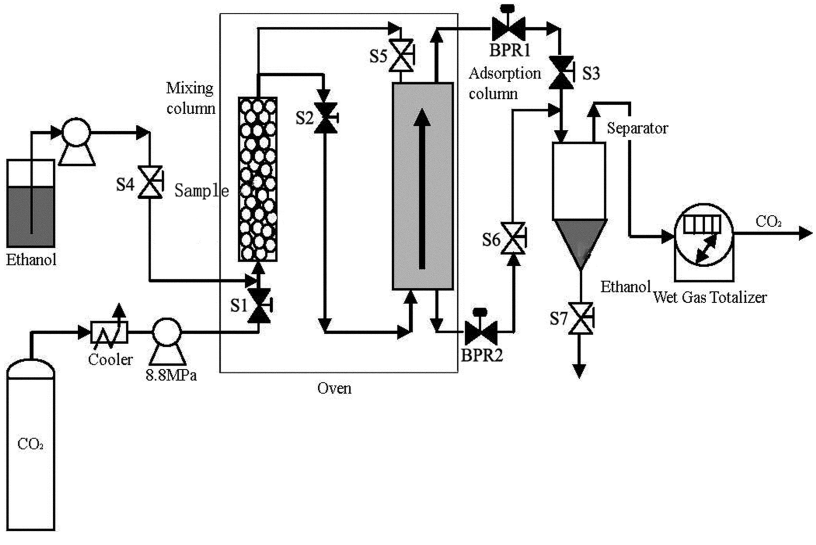

Figure 1. Experimental apparatus for the *Ligusticum* chuanxiong separation process.

dx.doi.org/10.1021/ie301274x | *Ind. Eng. Chem. Res.* 2012, 51, 14496−14502

$$-\varepsilon_i E_z \frac{\partial^2 c_i}{\partial z^2} + \frac{\partial}{\partial z}(\nu_1 c_i) + \varepsilon_i \frac{\partial c_i}{\partial t} + \rho_s \frac{\partial w_i}{\partial t} = 0 \quad (1)$$

where ε_i is the interparticle voidage; E_z is the axial dispersion coefficient; ν_i is the liquid-phase superficial velocity; ρ_s is the adsorbent bulk density; z and t are the axial coordinate and time, respectively; c_i is the molar concentration of component i; and w_i is the amount of component i adsorbed. In this simulation, it is assumed that the flow is modeled as convection with no dispersion, so $E_z = 0$. The mass balance equation then reduces to

$$\frac{\partial}{\partial z}(\nu_1 c_i) + \varepsilon_i \frac{\partial c_i}{\partial t} + \rho_s \frac{\partial w_i}{\partial t} = 0 \quad (2)$$

The kinetic model was calculated with the assumption of a linear lumped resistance. With linear lumped resistance selected, the mass transfer from the liquid phase to the solid phase is expressed by a linear-driving-force (LDF) model:

$$\frac{\partial w_i}{\partial t} = \mathrm{MTC}_i(w_i^* - w_i) \quad (3)$$

where w_i^* is the loading, which is in equilibrium with the liquid-phase composition. The overall mass-transfer coefficient (MTC_i) is given as a lumped parameter term comprising the resistance between the bulk liquid and the external adsorbents surface and the resistance exerted by the pore structure of the adsorbents.

The Extended Langmuir 1 isotherm is represented by the equation

$$w_i = \frac{\mathrm{IP}_{1i}\mathrm{IP}_{2i}c_i}{1 + \sum \mathrm{IP}_{2i}c_i} \quad (4)$$

where IP_{1i} and IP_{2i} are the Extended Langmuir 1 isotherm constants of component i.

The operating parameters for adsorption column in the model and the initial concentration of components in the feed are based on the experimental data (see Table 2).

Table 2. Operating Parameters for Adsorption

variable	value	description
Hb	0.072 m	height of adsorbent layer
Db	0.01 m	internal diameter of adsorbent layer
Ei	0.35 m^3 void/m^3 bed	interparticle voidage
Ep	0.4 m^3 void/m^3 bead	intraparticle voidage
RHOs	789 kg m^{-3}	bed density
MTC("B")	0.001 s^{-1}	constant mass-transfer coefficient
MTC("A")	0.01 s^{-1}	constant mass-transfer coefficient
IP(1,"B")	1.60×10^{-4}	isotherm parameter
IP(1,"A")	1.50×10^{-8}	isotherm parameter
IP(2,"B")	1190.31	isotherm parameter
IP(2,"A")	378686.40	isotherm parameter

3. RESULTS AND DISCUSSION

3.1. Extraction Using SC-CO_2. When the SC-CO_2 passed through the mixing column with the flow rate of 6.8×10^{-8} m^3/s (8.8 MPa, 328.15 K), the components were extracted from *Ligusticum* chuanxiong by SC-CO_2 to form the feed. Ferulic acid, z-ligustilide, and senkyunolide I had low solubilities ($<10^{-5}$ mol/mol) in SC-CO_2,[26] and the flow rate of SC-CO_2 was very low ($\sim 6.8 \times 10^{-8}$ m^3/s, 8.8 MPa, 328.15 K), so the concentration of ferulic acid, z-ligustilide, ligustrazine, and senkyunolide I in the feed could be considered to be constant within the experiment time. The concentrations of components in the feed were measured by HPLC with different time, and the average measured flow rates (C_{i0}) of ferulic acid, z-ligustilide, senkyunolide I, and ligustrazine in the feed were ~0.050, 1.325, 0.44, and 0.00024 mg/min, respectively.

3.2. Separation in SC-CO_2. *3.2.1. Measurement of Breakthrough Curves.* Figure 2a shows the breakthrough curves for ferulic acid, z-ligustilide, ligustrazine, and senkyunolide I at 8.8 MPa and 328.15 K. At 17 min, the concentration of ligustrazine in the effluent was equal to its initial concentration, and it explained that the breakthrough time of ligustrazine was ~17 min. The breakthrough times for the other three components were much longer. This indicates that ligustrazine was slightly adsorbed on the adsorbent, whereas ferulic acid, senkyunolide I, and z-ligustilide had large adsorption capacities on the adsorbent. The breakthrough curve of ligustrazine is steep, so it can be concluded that the mass-transfer coefficient for ligustrazine in SC-CO_2 in silica gel is quite large.

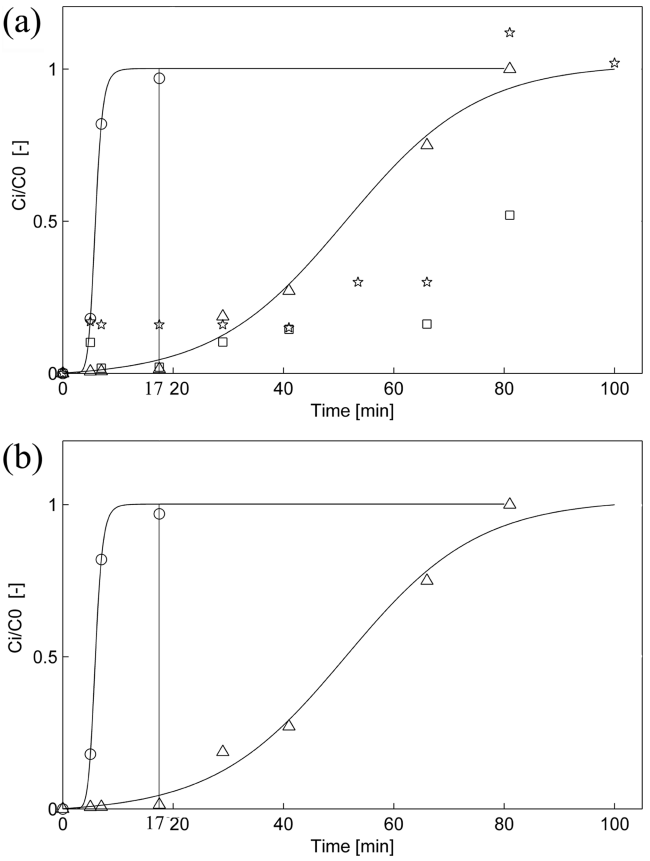

Figure 2. (a) Breakthrough curves of ferulic acid, z-ligustilide, ligustrazine, and senkyunolide I in the presence of SC-CO_2 at 328.15 K and 8.8 MPa: (circles, ○) ligustrazine, (stars, ☆) ferulic acid, (□) senkyunolide I, and (△) z-ligustilide. $C_{CO_2} = 6.8 \times 10^{-8}$ m^3/s, $C_{\text{ferulic acid}} = 0.050$ mg/min, $C_{\text{z-ligustilide}} = 1.325$ mg/min, $C_{\text{senkyunolide I}} = 0.44$ mg/min, and $C_{\text{ligustrazine}} = 0.00024$ mg/min). (b) Breakthrough curves for a quasi-binary system: (circles, ○) pseudo-component A and (triangles, △) pseudo-component B.

Since *Ligusticum* chuanxiong contains many components, it has a complicated adsorption behavior, because of multicomponent competitive adsorption. In order to analyze and

dx.doi.org/10.1021/ie301274x | Ind. Eng. Chem. Res. 2012, 51, 14496−14502

simulate the adsorption process, *Ligusticum* chuanxiong was assumed to be a quasi-binary system composed of slightly adsorbed pseudo-component A and strongly adsorbed pseudo-component B. Pseudo-component A includes ligustrazine, and the main components of pseudo-component B are lactones, such as senkyunolide I and z-ligustilide, and ferulic acid as a strongly adsorbed component is also included in pseudo-component B. The breakthrough curves for a quasi-binary system can be represented as shown in Figure 2b. The overall mass-transfer coefficient in the packed bed was estimated using empirical correlations, and coefficients having the magnitude of 0.01 (s^{-1}) for pseudo-component A and 0.001 (s^{-1}) for pseudo-component B were obtained.[7]

3.2.2. Adsorption Isotherm. The breakthrough curves for different feed concentration were measured; the adsorption amounts were calculated from the breakthrough curves. Then, the adsorption isotherm for components of *Ligusticum* chuanxiong in SC-CO_2 can be acquired by fitting the data. Figure 3 shows the adsorption isotherms of pseudo-components A and B in *Ligusticum* chuanxiong at 328.15 K and 8.8 MPa. Because of the different concentrations of the components in the feed, there was 4 orders of magnitude difference between pseudo-component A and pseudo-component B in adsorbed amounts.

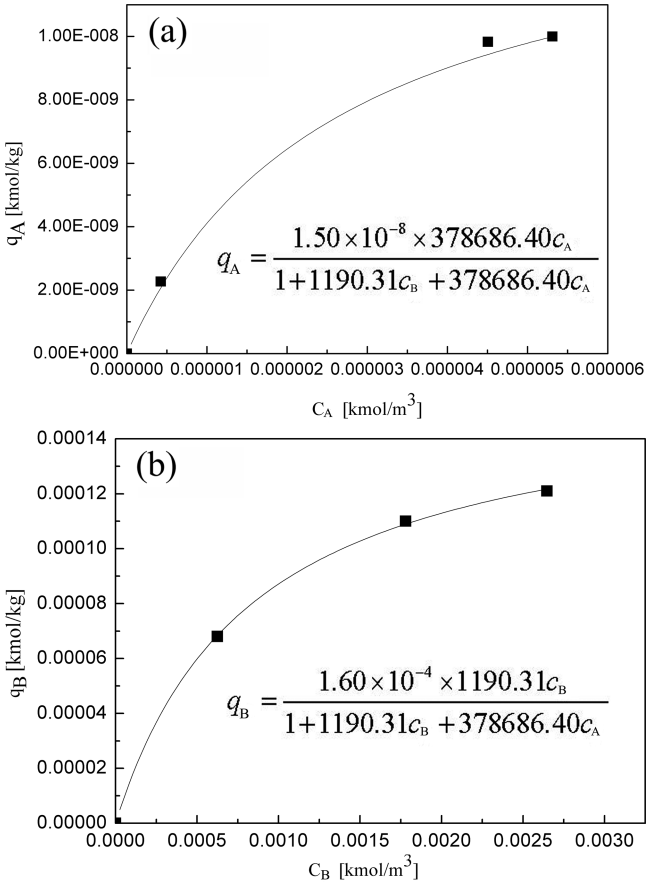

Figure 3. Adsorption isotherms for (a) pseudo-component A and (b) pseudo-component B on silica gel in the presence of SC-CO_2 at 328.15 K and 8.8 MPa.

The experimental data were correlated with the Extended Langmuir 1 isotherm equation (eq 4). The Extended Langmuir model was successfully used to fit experiment data, and this indicated that the components adsorbed on the silica gel belong to monolayer adsorption. In this quasi-binary system, values of $IP_{1A} = 1.50 \times 10^{-8}$ and $IP_{1A} = 378686.40$ were observed for pseudo-component A, and values of $IP_{1B} = 1.60 \times 10^{-4}$ and $IP_{2B} = 1190.31$ for pseudo-component B.

3.2.3. Breakthrough Curve Simulations. The process was modeled and simulated using Aspen Adsim adsorption software. The operating parameters for adsorption bed (see Table 2) and the initial concentration of components in the feed were based on the experimental data. The experimental breakthrough curves were predicted using the Extended Langmuir 1 adsorption isotherm equation, and comparisons between the experimental and simulated curves are shown in Figure 4. Pseudo-component A was only slightly adsorbed on the adsorbent and reached saturation after ~17 min. In contrast, pseudo-component B was the more selectively adsorbed component and the weakly adsorbed A was immediately eluted when it was present at a concentration higher than that in the feed. The shape of the breakthrough curves for pseudo-components A and B are quite different, because MTC = 0.01 (1/s) for pseudo-component A and MTC = 0.001 (1/s) for pseudo-component B. Figure 4 also indicates that the simulation model is adequate for the description of the process of fractionating *Ligusticum* chuanxiong by adsorption in SC-CO_2.

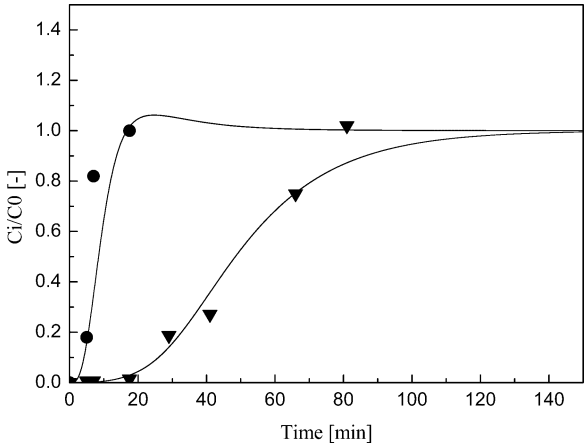

Figure 4. Comparison of simulated and experimental breakthrough curves (curves represent data simulated with Aspen Adsim, and symbols represent experimental data ((circles, ○) pseudo-component A and (triangles, △) pseudo-component B).

3.3. Effect of Adsorption Time. The effect of adsorption time was considered in order to design a cycle process for the fractionation of *Ligusticum* chuanxiong. Figure 5 shows the recovery and concentration ratio (A/B) of pseudo-component A in the effluent, as a function of adsorption time at an adsorption pressure of 8.8 MPa and a temperature of 328.15 K. The concentration ratio of pseudo-component A in the effluent decreased with time and the recovery of A increased. The product recovery (1.9%) for an adsorption time of 300 s was much lower than that (65.6%) for an adsorption time of 1050 s, whereas the concentration ratio of pseudo-component A decreased from 272 to 60. Thus, the adsorption time can be adjusted according to the product requirements. The curves in Figure 5 clearly demonstrate good agreement between the experimental data and the simulated results.

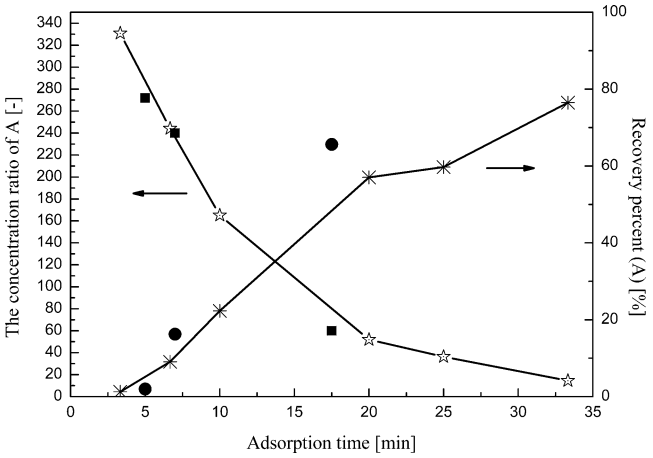

Figure 5. Effect of adsorption time on concentration ratio and recovery (curves represent simulated data, and symbols represent experimental data (squares, ■) concentration ratio of A, and (circles, ●) recovery percentage).

3.4. Effect of the Flow Rate of the Strippant. Increasing the pressure of SC-CO_2 or adding a strippant (such as ethanol, acetic ether, or benzene) is the common method for regenerating adsorbents.[8] In this work, SC-CO_2 containing 5% (molar mass) ethanol was used to elute A and B, which were adsorbed on the adsorbent.

Three flow rates of strippant were used to the regenerate adsorbent: $F = 6.9 \times 10^{-8}$ m^3/s, $F = 1.24 \times 10^{-7}$ m^3/s, and $F = 8.0 \times 10^{-7}$ m^3/s (8.8 MPa, 328.15 K). In Figure 6, the symbols represent the experimental concentration of components measured via HPLC at different desorption times, and the curves are the simulation desorption lines. The experimental data (denoted by symbols in Figure 6) are well-distributed around the simulation curves, which showed that the simulation results described the experimental data well. Both pseudo-components A and B were desorbed by SC-CO_2 that contained 5% ethanol and the regeneration became more complete and occurred more quickly as the flow rate of the strippant increased. Pseudo-component A was desorbed more easily and was regenerated within 20 min at a lower flow rate of the strippant, whereas for pseudo-component B, ~30 min were needed for regeneration, even at a flow rate of 8.0×10^{-7} m^3/s (8.8 MPa, 328.15 K). Thus, for cycle operations, the flow rate of strippant was selected as 8.0×10^{-7} m^3/s (8.8 MPa, 328.15 K), and the desorption time was 2000 s.

3.5. A Cycle Simulation. Figure 7 shows the concentration curves of each component in the effluent during the adsorption and desorption steps for the first four simulated cycles (F_{D1} = 8.0×10^{-7} m^3/s 8.8 MPa, 328.15 K). The curves in Figure 7a at times $a \times 2000$ to $a \times 2000 + 2000$ s (where $a = 0, 2, 4, 6$) are breakthrough adsorption curves and the curves in Figure 7b at times $b \times 2000$ to $b \times 2000 + 2000$ s (where $b = 1, 3, 5, 7$) are desorption curves. At the beginning of the adsorption, the bed reached to the adsorption pressure using SC-CO_2, and no components were adsorbed on the silica gel. Pseudo-components A and B were adsorbed on the silica gel during the adsorption step and the breakthrough curves in Figure 7a are the same as Figure 4. During the desorption step, the adsorbed components were eluted from the adsorbent, but the adsorbent could not be completely regenerated. This also means that a few components were not eluted from the adsorbent in the subsequent cycles. Therefore, the adsorption

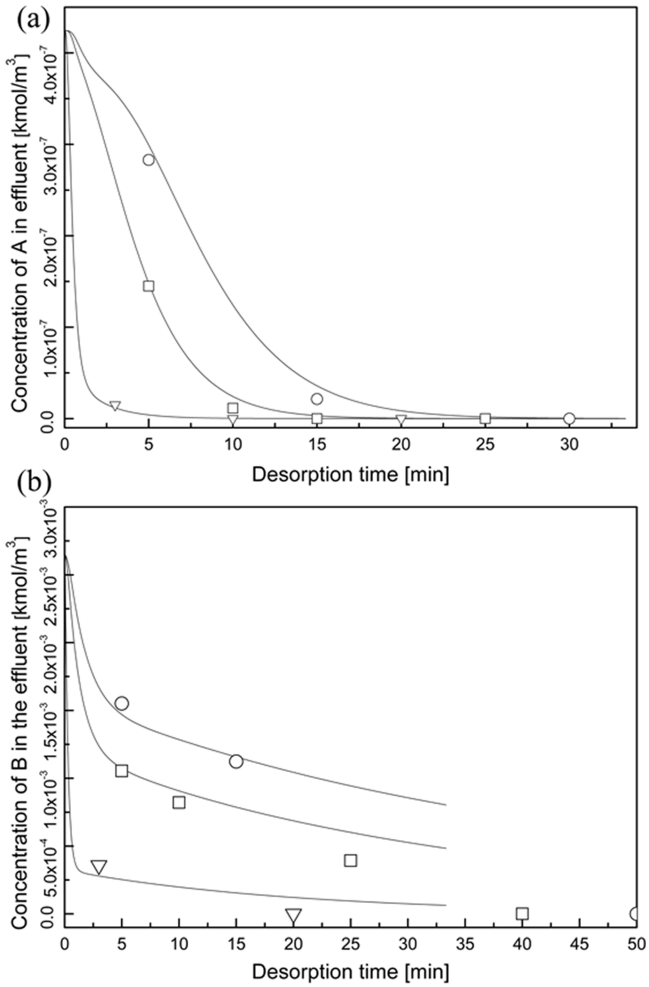

Figure 6. Desorption curve at different flow rates of strippant (curves represent the simulated data, and symbols represent experimental data ((circles, ○) $F_D = 6.9 \times 10^{-8}$ m^3/s, (squares, □) $F_D = 1.24 \times 10^{-7}$ m^3/s, and (triangles, △) $F_D = 8.0 \times 10^{-7}$ m^3/s).

capacities of the adsorbent were lower than those of the fresh adsorbent. This affected the time at which pseudo-component B started to appear in the effluent during the adsorption step; pseudo-component B appeared later in the first cycle than in later cycles (see Figure 7). When the adsorption process was repeated, the adsorption bed reached a steady state, so the shapes of the breakthrough curves in each cycle are almost the same.

For the cycle simulation, the amount of A and B adsorbed on the adsorbent varied with adsorption time and with the axial distance along the bed as shown in Figure 8. At the beginning of the adsorption step, the components first came in contact with the adsorbent at the front of the column and adsorbed there, so the amount of adsorbed B decreased along the column (see Figure 8b). A competitive multicomponent adsorption behavior is also observed in Figure 8, i.e., the strongly adsorbed pseudo-component B was preferentially adsorbed on the adsorbents. This means that more B was adsorbed at the front of the bed than A, and the amount of A adsorbed at the front of the column was much lower than at the end. Figures 8a and 8b show that the amount of A and B adsorbed on the adsorbent increased with time. During the desorption step, the amount of A and B adsorbed on the adsorbent decreased with time. Because the strippant passed through the adsorption bed

dx.doi.org/10.1021/ie301274x | Ind. Eng. Chem. Res. 2012, 51, 14496−14502

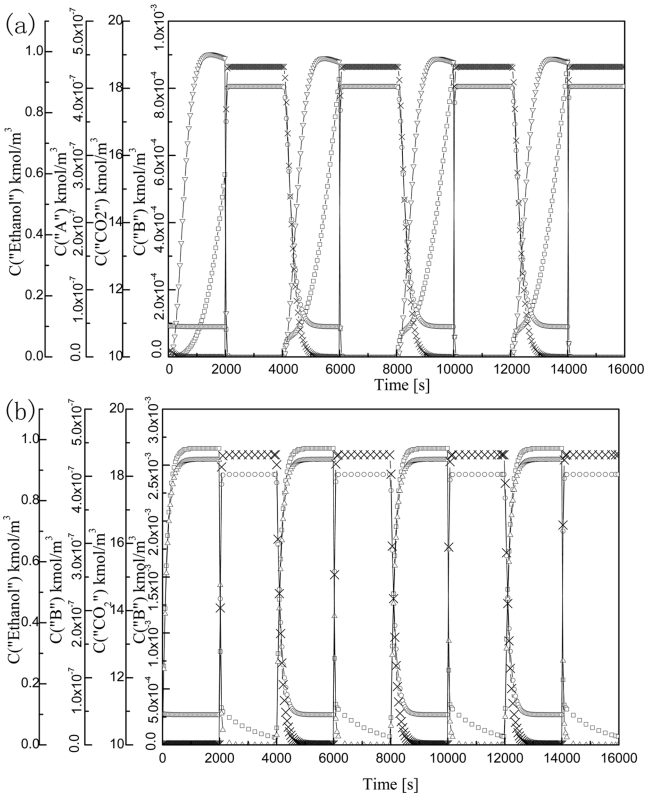

Figure 7. Concentration curves for each component in the effluent during (a) the adsorption step and (b) the desorption step for the first four simulated cycles (F_{D1} = 8.0 × 10^{-7} m^3/s ((circles, ○) CO_2, (triangles, ▽ and △) pseudo-component A, (squares, □) pseudo-component B, and (forks, ×) ethanol).

from back to front, pseudo-component B adsorbed at the end of the adsorption bed was eluted more quickly. Pseudo-component A, as the more weakly adsorbed component, was eluted from the adsorbent more rapidly. Pseudo-component A was completely eluted from the adsorbent, whereas a small amount of pseudo-component B still remained on the adsorbent after the desorption operation.

5. CONCLUSIONS

Multicomponent adsorption experiments of *Ligusticum* chuanxiong were investigated using commercial pellets of silica gel as the adsorbent. The weakly adsorbed pseudo-component A and the strongly adsorbed pseudo-component B were successfully obtained in the adsorption and desorption step, and a high concentration ratio of B (the recovery of 85%) was obtained after the desorption step. The effects of the adsorption times, and the flow rate of the strippant, on the concentrations of the components in the effluent and the recovery of the products were also investigated.

Aspen Adsim software was used to simulate the adsorption process. Comparison of the experimental data with the simulation results found that the single bed simulation roughly agreed with the experimental data. Thus, Aspen Adsim is a very useful tool for simulating the adsorption dynamics of complex mixtures in supercritical CO_2 (SC-CO_2). Based on this, a continuous cyclic operation was simulated by Aspen Adsim, and the amount of adsorbed components on the adsorbents was predicted graphically. These simulations are helpful for obtaining more-accurate predictions and improving experiments. However, there are few data of adsorption equilibrium and kinetics for traditional Chinese medicine (TCM) components in supercritical fluid chromatography (SFC) in the literature that prevent the development of new adsorption models. Thus, there is a desperate need to build an adsorption database for TCM components to different adsorbents in SFC.

AUTHOR INFORMATION

Corresponding Author

*Tel.: +086-022-27892097. E-mail: donghuizhang@tju.edu.cn.

Notes

The authors declare no competing financial interest.

ACKNOWLEDGMENTS

This work was supported by the program of Introducing Talents of Discipline to Universities, China (Grant No. 06006).

REFERENCES

(1) Hou, Y. Z.; Yang, J.; Zhao, G. R.; Yuan, Y. J. Ferulic acid inhibits vascular smooth muscle cell proliferation induced by angiotensin II. *Eur. J. Pharmacol.* **2004**, *499*, 85−90.

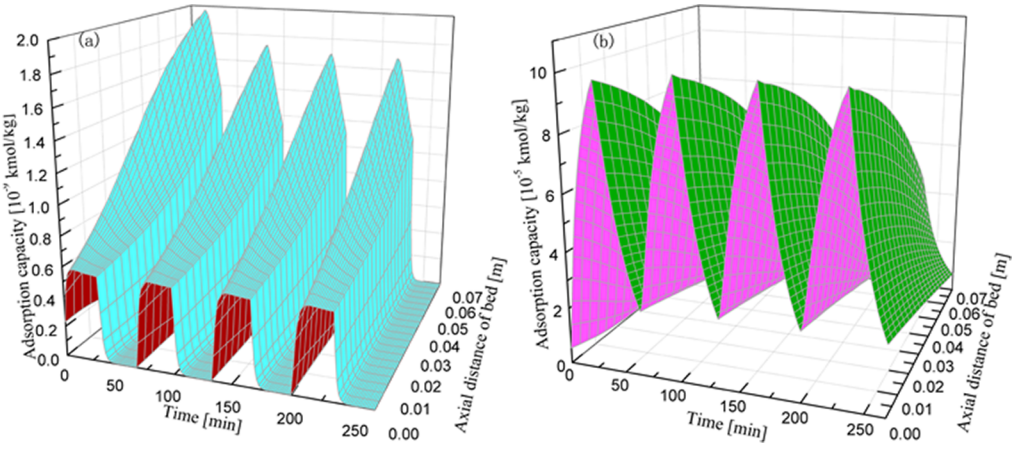

Figure 8. Adsorption capacity distribution along time and axial distance (first four simulated cycles): (a) pseudo-component A and (b) pseudo-component B.

(2) Zschocke, S.; Liu, J. H.; Stuppner, H.; Bauer, R. Comparative study of roots of Angelica sinensis and related umbeliferous drugs by thin layer chromatography, high-performance liquid chromatography, and liquid chromatography−mass spectrometry. *Phytochem. Anal.* **1998**, *9*, 283−290.
(3) Li, H. X.; Ding, M. Y.; Yu, J. Y. Separation and identification of the phthalic anhydride derivatives of *ligusticum* chuanxiong hort by GC-MS, TLC, HPLC-DAD, and HPLC-MS. *J. Chromatogr. Sci.* **2002**, *40*, 156−161.
(4) Li, H. X.; Ding, M. Y.; Yu, J. Y. Separation and determination of ephedrine alkaloids and tetramethylpyrazine in *ephedra sinica* stapf by gas chromatography−mass spectrometry. *J. Chromatogr. Sci.* **2001**, *39*, 370−374.
(5) Ong, E. S.; Woo, S. O. Determination of aristolochic acids in medicinal plants (Chinese) prepared medicine using capillary zone electrophoresis. *Electrophoresis* **2001**, *22*, 2236−2241.
(6) Chen, X. G.; Liang, K.; Su, X. Y.; Fu, H. J.; Ni, J. Y.; Zhao, R. H.; Zou, H. F. Separation and identification of compounds in *Rhizoma* chuanxiong by comprehensive two-dimensional liquid chromatography coupled to mass spectrometry. *J. Chromatogr. A* **2004**, *1040*, 169−178.
(7) Sate, M.; Goto, M.; Kodama, A.; Hirose, T. New fractionation process for citrus oil by pressure swing adsorption in supercritical carbon dioxide. *Chem. Eng. Sci.* **1998**, *53*, 4095−4104.
(8) Bracey, W.; Akman, U.; Sunol, A. K. High pressure adsorption and supercritical desorption of aqueous fructose-glucose mixture. *J. Supercrit. Fluids* **1991**, *4*, 60−68.
(9) Subra, P.; Vega-Bancel, A.; Reverchon, E. Breakthrough curves and adsorption isotherms of terpene mixtures in supercritical carbon dioxide. *J. Supercrit. Fluids* **1998**, *12*, 43−57.
(10) Iwai, Y.; Uchida, H.; Mori, Y.; Higashi, H.; Matsuki, T.; Furuya, T.; Arai, Y.; Yamamoto, K.; Mito, Y. Separation of isomeric Dimethylnaphthalenes mixture in supercritical carbon dioxide by using zeolite. *Ind. Eng. Chem. Res.* **1994**, *33*, 2157−2160.
(11) Uchida, H.; Iwai, Y.; Amiya, M.; Arai, Y. Adsorption behaviors of 2,6- and 2,7-Dimethylnaphthalenes in supercritical carbon dioxide using NaY-type zeolite. *Ind. Eng. Chem. Res.* **1997**, *36*, 424−429.
(12) Uchida, H.; Iwai, Y.; Nitta, M.; Arai, Y. Impulse Response Analysis for Adsorption of 2,6- and 2,7-Dimethylnaphthalenes in supercritical carbon dioxide using NaY-type zeolite. *Ind. Eng. Chem. Res.* **1998**, *37*, 595−598.
(13) Iwai, Y.; Higuchi, M.; Nishioka, H.; Takahashi, Y.; Arai, Y. Adsorption of supercritical carbon dioxide + 2,6- and 2,7-Dimethylnaphthalene isomers on NaY-type zeolite. *Ind. Eng. Chem. Res.* **2003**, *42*, 5261−5267.
(14) Lim, S.; Rizvi, S. S. H. Adsorption and desorption of cholesterol in continuous supercritical fluid processing of anhydrous milk fat. *J. Food Sci.* **1996**, *61*, 817−820.
(15) Mohamed, R. S.; Neves, G.; Kieckbusch, T. G. Reduction in cholesterol and fractionation of butter oil using supercritical CO_2 with adsorption on alumina. *Int. J. Food. Sci. Technol.* **1998**, *33*, 445−454.
(16) Goto, M.; Fukui, G.; Wang, H. T.; Kodama, A.; Hirose, T. Deterpenation of bergamot oil by pressure swing adsorption in supercritical carbon dioxide. *J. Chem. Eng. Jpn.* **2002**, *35*, 372−376.
(17) Wang, H. T.; Goto, M.; Sasaki, M.; Hirose, T. Separation of Separation of α-tocopherol and squalene by pressure swing adsorption in supercritical carbon dioxide. *Ind. Eng. Chem. Res.* **2004**, *43*, 2753−2758.
(18) Shen, Z.; Mishra, V.; Imison, B.; Palmer, M.; Fairclough, R. Use of adsorbent and supercritical carbon dioxide to concentrate flavor compounds from orange oil. *J. Agric. Food Chem.* **2002**, *50*, 154−160.
(19) Brunner, G.; Johannsen, M. New aspects on adsorption from supercritical fluid phases. *J. Supercrit. Fluids* **2006**, *38*, 181−200.
(20) Lubbert, M.; Brunner, G.; Johannsen, M. Adsorption equilibria of α- and δ-tocopherol from supercritical mixtures of carbon dioxide and 2-propanol onto silica by means of perturbation chromatography. *J. Supercrit. Fluids* **2007**, *42*, 180−188.
(21) Su, B. G.; Xing, H. B.; Han, Y. S.; Yang, Y. W.; Ren, Q. L.; Wu, P. D. Adsorption equilibria of *cis*-5,8,11,14,17-eicosapentaenoic acid ethyl ester and *cis*-4,7,10,13,16,19-docosahexaenoic acid ethyl ester on C18-bonded silica from supercritical carbon dioxide. *J. Chem. Eng. Data* **2009**, *54*, 2906−2913.
(22) Barcia, P. S.; Silva, J. A. C.; Rodrigues, A. E. Adsorption dynamics of C5−C6 isomerate fractions in zeolite beta for the octane improvement of gasoline. *Energy Fuels* **2010**, *24*, 1931−1940.
(23) Kim, J. K.; Natarajan, G.; Wankat, P. C. Focusing in liquid thermal adsorption system. *Adsorption* **2003**, *9*, 117−123.
(24) Barcia, P. S.; Silva, J. A. C.; Rodrigues, A. E. Octane upgrading of C5/C6 light naphtha by layered pressure swing adsorption. *Energy Fuels* **2010**, *24*, 5116−5130.
(25) Yang, S. l.; Choi, D. Y.; Jang, S. C.; Kim, S. H.; Choi, D. K. Hydrogen separation by multi-bed pressure swing adsorption of synthesis gas. *Adsorption* **2008**, *14*, 583−590.
(26) Ru, Y.; Li, S. L.; Chung, H. S.; Tam, Y. K.; Ge, L. Simultaneous quantification of 12 bioactive components of *ligusticum* chuanxiong hort. by high-performance liquid chromatography. *J. Pharm. Biomed. Anal.* **2005**, *37*, 87−95.
(27) Sun, Y.; Li, S.; Quan, C. The measurement of the solubility of ferulic acid and tetramethylpyrazine in supercritical carbon dioxide. *J. Chem. Eng. Chin. Univ.* **2005**, *6*, 839−842.